Characterization of Advanced Hybrid Rocket Engines

Anna Petrarolo⋆*, Mario Kobald*⋆ *and Christian Schmierer*⋆,⋆⋆
⋆ *DLR, Institute of Space Propulsion*
Langer Grund, 74239 Hardthausen, Germany
⋆⋆*Institute of Space Systems, University of Stuttgart*
Pfaffenwaldring 29, 70569 Stuttgart, Germany

Abstract

In the last years, the discovery of high regression rate liquefying fuels has generated a renewed interest in hybrid propulsion systems due to some advantages in certain applications compared to solid or liquid rockets. The intrinsic safety, simplicity and low cost make hybrid systems appreciable for research at university level. At the University of Stuttgart a 500 N hybrid rocket engine, called MIRAS (MIcro RAkete Stuttgart), has been developed by the student team HyEnD (Hybrid Engine Development) within the DLR STERN (STudentische Experimental RaketeN) program. MIRAS is propelled by a liquefying paraffin-based solid fuel and nitrous oxide as oxidizer. It was designed as a technology demonstrator for a scale-up version with a thrust of 10000 N. The test campaign was conducted with an experimental set-up at the test bench M11.5 at the DLR Lampoldshausen. A ballistic characterization of paraffin-based hybrid rocket fuels with different additives in combination with nitrous oxide and a performance evaluation of the 500 N hybrid rocket engine are carried out. A wide range of operating conditions, fuel compositions, injector geometries and engine configurations are evaluated with this engine. Effects of different injector geometries and post combustion chamber designs on the engine performance are analyzed. Additionally, the appearance of combustion instabilities under certain conditions is described, their effect and possible mitigation techniques are also investigated.

1. Introduction

Hybrid Engine Development (HyEnD) is a student team located at the University of Stuttgart, since its foundation in 2006. In the years from 2006 to 2012, HyEnD focused on developing its own hybrid rocket engines in different scales from 250 N to 2000 N thrust [1]. In 2012 the project Studentische Experimentalraketen (student experimental rockets, STERN, [2]) was initiated by the German Aerospace Center (DLR) and HyEnD applied for it with the Institute of Space Systems. The gained experience and knowledge of HyEnD in ground testing hybrid rocket engines was the baseline to develop, construct and build its own experimental hybrid sounding rocket within the 3 years of the STERN project. In September 2012 the rocket development began, starting from scratch. Except for the rocket engine, HyEnD had only little experience with the rocket systems including flight-weight propellant management, rocket recovery and flight electronics. Within the first year, the concept of the rocket called HEROS (Hybrid Experimental ROcket Stuttgart) was developed. Simultaneously, a smaller demonstrator rocket called MIRAS (Micro Rakete Stuttgart) was initiated in order to test all subsystems in a smaller scale before the launch of HEROS in 2015. HEROS was targeted to have a thrust of 10 kN and maximum altitude of higher than 20 km. A smaller scale was applied for MIRAS. It can reach altitudes of around 2 km with a 500 N engine. This allows to test the rocket on German launch sites. Both MIRAS and HEROS use a hybrid rocket engine with a paraffin-based fuel and liquid nitrous oxide as oxidizer. More than 140 hot-fire tests have been performed in the HyEnD project so far. Results of the 500 N engine development are presented here and the 10 kN test campaign is presented in [3]. A lot of the subsystems that will be used on HEROS could be built and tested in smaller scale for MIRAS. This includes the flight-weight rocket engine, the pyrotechnical valve, the oxidizer tank, the recovery system, the flight electronics and the Ground Support Equipment (GSE). During the development of the MIRAS demonstrator, a lot of improvements could be made to the design of the different subsystems which could be applied to the HEROS rocket design until the end of the second year. At that time HyEnD also passed the Critical Design Review. The review board included experts from the DLR MORABA, the DLR Space Agency and the DLR Institute of Space Propulsion. In early 2015 the MIRAS demonstrator rocket was launched successfully, proving that the baseline concept is working. In Summer 2015 a second flight of MIRAS is planned before the launch campaign of HEROS in October 2015. It is planned to take place at the Esrange Space Center near Kiruna, Sweden. The latest project advancement was the successful Integration Progress Review in May 2015.

A hybrid rocket engine is somehow placed between solid motors and liquid engines since the propellants are stored in two different states of matter, solid and liquid (or gaseous). In general, the liquid oxidizer is stored in a pressurized tank, like in a liquid system, while the solid fuel grain is placed in the combustion chamber, like in a solid motor. The oxidizer is injected into the head end of the combustion chamber where it reacts with the fuel vapours in the fluid-dynamic boundary layer developed along the surface of the solid fuel. The burning reactions are completed in a post combustion chamber. The reaction products are then accelerated through a gas-dynamic nozzle in order to generate the thrust. Hybrid rocket engines combine the advantages of solid and liquid propulsion systems: simple and safe storability due to the separately stored oxidizer and fuel, possibility of throttling and immediate shut-down by closing the oxidizer's main valve and control of the mixture ratio by variation of the oxidizer mass flow.

2. Combustion Tests Analysis

A test campaign of 86 hot fire ground tests was carried out during the months from September 2013 to July 2014 at the test bench M11.5 at DLR Lampoldshausen. Cylindrical paraffin-based fuel samples with a single central port perforation were tested in combination with nitrous oxide. The chamber pressure was about 30-35 bar and the expansion ratio of the engine was 5.

The space-time averaged regression rate and all the averaged performance were computed using measurements taken from different pressure transducers, a flow-meter and a load cell. All the fuel grains were measured and weighted before and after each test. Theoretical performance was computed with the NASA program CEA (Chemical Equilibrium with Applications). Combustion stability was evaluated by using Fast-Fourier Transformations and spectrograms of the pressure signals.

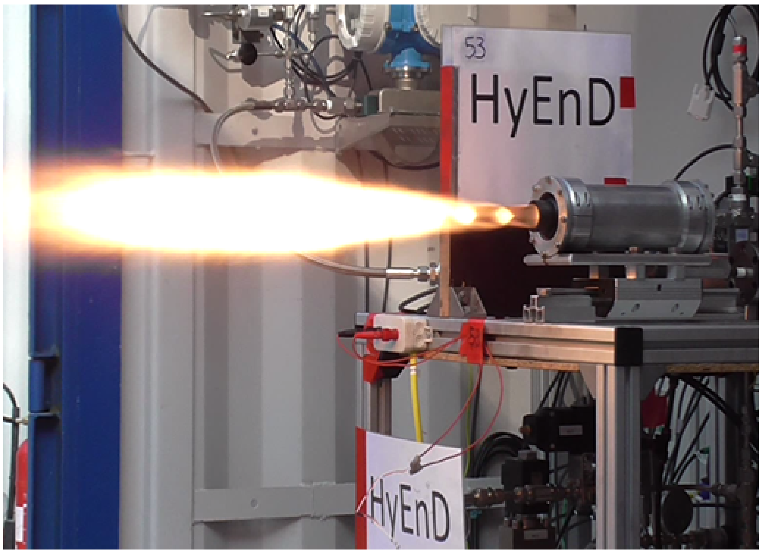

Figure 1: Hot fire testing

2.1 Regression Rate and Performance Analysis

Due to the two-phase propellant configuration, hybrid systems are characterized by a combustion limited by diffusion. This makes the fuel regression rate and the performance primarily dependent on the fluid-dynamics in the combustion chamber and on the oxidizer mass flux, which is changing during the combustion process. For this reason, hybrids are characterized by time-varying regression rate and performance. According to the classic formula derived by Marxman [4], the hybrid regression rate is dependent on the total mass flux in the port G (which, in turn, depends on the time-varying port diameter), port length coordinate x and three ballistic coefficients a, n, m, according to Equ. 1.

$$\dot{r} = aG^n x^m \tag{1}$$

Usually, the total mass flux is replaced by the oxidizer mass flux G_{Ox}. Moreover, in this analysis, the longitudinal variation in the regression rate will be ignored by assuming a simple average value in space considering $m = 0$. Thus, the regression rate formula becomes

$$\dot{r} = a{G_{Ox}}^{n} \tag{2}$$

The aim of the regression rate analysis is to experimentally determine the ballistic coefficients for each fuel and oxidizer combination. Due to the discrete nature of fuel mass measurements, averaging both in space and time is necessary. Unfortunately, the methods of data reduction are not unique because of the non-linear nature of the problem and each method can produce significantly different results. In this analysis the space-time averaged regression rate as defined by Karabeyoglu et al. [5] was used. For each test the average regression rate was estimated from initial port diameter and burned fuel mass measurements, using Equ. 3.

$$\bar{\dot{r}} = \frac{D_f - D_i}{2t_b} \tag{3}$$

The initial diameter D_i is easily measured before each test. The final space-averaged diameter D_f should be computed by measuring the port diameter as a function of the chamber longitudinal coordinate and taking an average value. In this analysis D_f was computed according to Equ. 4.

$$D_f = \left[\frac{4(m_{fuel_i} - m_{fuel_f})}{\pi\rho_{fuel}L_{fuel}} + {D_i}^2\right]^{\frac{1}{2}} \tag{4}$$

For the computation of the oxidizer mass flux, different averaging techniques are available due to the non-linear nature of the flux formula. In this analysis, the space-averaged oxidizer mass flux based on the averaged port diameter was used according to Equ. 5. The diameter averaging method, which is a simple arithmetic average of the initial and final port diameters, produces the smallest averaging induced error [5].

$$\overline{G}_{Ox} = \frac{16\overline{\dot{m}}_{Ox}}{\pi(D_i + D_f)^2} \tag{5}$$

For the computation of the average engine performance the following relations were used, respectively for the characteristic velocity c^* (Equ. 6) and the specific impulse I_{sp} (Equ. 7):

$$\overline{c^*} = \frac{\overline{P}_c A_t}{(\overline{\dot{m}}_{Ox} + \overline{\dot{m}}_f)} C_d \tag{6}$$

$$\overline{I}_{sp} = \frac{\bar{F}}{(\overline{\dot{m}}_{Ox} + \overline{\dot{m}}_f) g_0} \tag{7}$$

where $\overline{P}_c$ is the average chamber pressure, $\overline{\dot{m}}_{Ox}$ and $\overline{\dot{m}}_f$ are the average oxidizer and fuel mass flow rate, $\bar{F}$ is the average thrust, A_t is the nozzle throat area, C_d is the nozzle discharge coefficient taken as 0.99 for all tests and $g_0 = 9.81\ \frac{\mathrm{m}}{\mathrm{s}^2}$ is the gravitational acceleration.

For efficiencies computation, the average performance was compared with theoretical values obtained with the software NASA CEA, evaluated at the average chamber pressure $\overline{P}_c$ and mixture ratio $\overline{OF} = \overline{\dot{m}}_{Ox}/\overline{\dot{m}}_f$ by setting equilibrium conditions. An expansion ratio of 5 was used in the computations.

2.2 Error Analysis

An error analysis was conducted in order to quantify the uncertainties in the computed variables. There are two kinds of errors, which have to be combined to estimate the total error:

- *systematic errors*, which are introduced by using a particular time averaging method. They are constant in repeated measurements under fixed operating conditions, thus causing an offset in the estimation of the true value of the measured variable. According to the error analysis conducted by Karabeyoglu et al. [5], there is no systematic error for the regression rate and performance estimation, while the systematic error for the oxidizer mass flux is obtained as a function of the diameter ratio $R = D_f/D_i$ and mass flux exponent n according to Equ. 8.

$$E_{syst_G} = \frac{4}{(2n+1)^{\frac{1}{n}}}\left[\frac{R^{2n+1}-1}{(R+1)^{2n}(R-1)}\right]^{\frac{1}{n}} \tag{8}$$

- *random errors*, which are associated with the measurements. They are introduced through the repeatability and resolution of the measurement system components, calibration, measurement procedure and technique by temporal and spatial variations of the measured variables and variations in the process operating and environmental conditions. They manifest themselves as scatter of the measured data and typically they decrease with increasing number of tests. For the computation of random errors it is necessary to consider the propagation of the measurement errors when uncertain values are used to define other quantities. A method used to estimate the uncertainty in a variable that depends on other uncertain values is the *RSS method (square Root of the Sum of the Squares)* weighted on the first derivatives. The same results of Karabeyoglu et al. [5] were obtained for errors in $\dot{r}$ and G_{Ox} estimation.

$$E_{rand_r} = \sqrt{\left(\frac{R}{R-1}E_{D_f}\right)^2 + \left(\frac{1}{R-1}E_{D_i}\right)^2 + E_t^2} \tag{9}$$

$$E_{rand_G} = \sqrt{\left(\frac{2R}{R+1}E_{D_f}\right)^2 + \left(\frac{2}{R+1}E_{D_i}\right)^2 + E_{\dot{m}_{Ox}}^2} \tag{10}$$

For the computation of the total error it is necessary to combine the systematic and random errors by using the *RSS method*:

$$E_{tot} = \sqrt{E_{syst}^2 + E_{rand}^2} \tag{11}$$

2.3 Frequency Analysis

In order to better understand what happens in the combustion chamber during the burning process, a spectral analysis of the chamber pressure was carried out with MATLAB® using the Signal Processing Toolbox.
Pressure data were windowed through a rectangular or Hanning window with the purpose of minimizing the spectral leakage, for the calculation of the spectra over the entire firing. Then a Fast Fourier Transform (FFT) was performed to display the overall spectrum. In order to reduce the noise, a moving average and an auto-spectrum were performed for each test. A *Power Spectral Density (PSD)*, using the MATLAB "Pwelch" routine, was also applied to the pressure data. A spectrogram was used to get a better overview of the frequencies resolved over time.

3. Combustion Instability

From a general point of view, *smooth combustion* occurs when pressure oscillations during steady operation do not exceed ±5% of the mean chamber pressure. Combustion that gives greater pressure fluctuations which occur at random intervals is called *rough combustion*. Combustion is defined to be unstable when the fluctuations in the chamber pressure exceed more than ±5 − 10% of the mean pressure value and it is characterized by oscillations occurring at well-defined time intervals [6]. These oscillations can cause an energy transfer from the combustion to the acoustic modes of the chamber, which can lead to different failure mechanisms due to the increase in chamber pressure or heat transfer to the walls. Fortunately, the combustion chamber pressure oscillations observed in hybrid systems are limited in amplitude and typically are not able to produce catastrophic consequences. This is most likely due to the non-premixed diffusion controlled flame which makes the regression rate not pressure dependent. However, oscillatory combustion in hybrids could still generate structural/thermal loading, thrust oscillations and high regression rate (DC shift) which could lead to unplanned thinning of the fuel web and the insulation material. From a general point of view, strong instabilities have to be avoided because they can cause excessive mechanical vibrations on the structure; on the other hand, mild instabilities may improve combustion efficiency by promoting mixing between fuel and oxidizer. Combustion instabilities in hybrid rocket engines can be classified into:

- **Non-acoustic instabilities**: they are usually characterized by low-frequency chamber pressure fluctuations and low intensity. Typically, they are caused by a coupling between the oxidizer mass flow in the feed system and the combustion process, chuffing of the solid fuel, coupling between the atomization/vaporization lags of the liquid oxidizer and the combustion and gasdynamic processes in the chamber, pressure sensitivity of the combustion (only at very high and low oxidizer mass flux regimes) or vortex-shedding in the pre- or post-combustion chamber. Carmicino [8] gives two relations for computing the frequency of the *vortex shedding instabilities* in the pre and post combustion chamber for a cylindrical fuel sample with a single central port perforation:

$$f_{VS-pre} = Sr\frac{4\dot{m}_{Ox}R_{Ox}T_{Ox}}{\pi D_f^3 P_c} \tag{12}$$

where $Sr = \dfrac{fD}{U}$ (f is the frequency of vortices detachment, D is the characteristic length, U is the velocity of the fluid) is the Strouhal number that varies in the range of $0.25 \leq Sr \leq 0.5$ [8], $\dot{m}_{Ox}$ is the oxidizer mass flow rate, R_{Ox} is the specific gas constant of the oxidizer, T_{Ox} is the oxidizer temperature, D_f is the inner diameter of the fuel grain, P_c is the chamber pressure.

$$f_{VS-post} = \eta_{c^*} c^*_{th} \psi^2_{th} Sr \frac{D_t^2}{D_f^3} \tag{13}$$

where η_{c^*} is the combustion efficiency, D_t is the nozzle throat diameter and $\psi_{th} = \left[\gamma\left(\dfrac{2}{\gamma+1}\right)^{\frac{\gamma+1}{\gamma-1}}\right]^{\frac{1}{2}}$ is a function of the isentropic exponent.

The typical non-acoustic combustion instabilities for hybrids are the *intrinsic low-frequency instabilities*, which are associated with the boundary layer combustion process. It is observed for both liquid and gaseous oxidizers. According to Karabeyoglu et al. [9], these instabilities are based on a complex coupling between thermal transients in the solid fuel, wall heat transfer blocking and the transients in the boundary layer. The empirical formula for this frequency is [9]:

$$f_{ILF} = \frac{0.48}{\tau_{bl}} = 0.2341\left(2 + \frac{1}{OF}\right)\frac{G_{Ox}(RT)_{av}}{L_{fuel}P_c} \tag{14}$$

where OF is the mixture ratio, G_{Ox} is the oxidizer mass flux, $(RT)_{av} = 4.47 \cdot 10^5$ is a constant depending on the oxidizer and fuel, L_f is the fuel length, P_c is the chamber pressure and τ_{bl} is the boundary layer delay time.

- **Acoustic Instabilities**: these oscillations are characterized by higher frequencies and amplitudes with respect to the non-acoustic ones. They often coexist or can be triggered by the low frequency instabilities. Typical acoustic modes are the *Helmholtz mode* (also known as the bulk mode), which is related with the gas motion in and out of the nozzle, and the *longitudinal acoustic modes of the chamber*. According to Carmicino [8], they are defined as:

$$f_H = \frac{c}{2\pi}\sqrt{\frac{A_t}{V(l+0.8D_t)}} \tag{15}$$

where c is the average speed of sound in the chamber, A_t is the nozzle throat area, l is the exhaust nozzle length and V is the combustion port total volume, that is the sum of the pre-chamber, fuel port and post-chamber volumes.

$$f_{1L} = \frac{c}{2L} = \sqrt{\frac{\gamma(RT)_{av}}{2L}} \tag{16}$$

where L is the total combustion chamber length.

The stability of a hybrid rocket engine is closely linked to the injectors geometry and to the configuration of the pre-combustion chamber. Lots of researches have been done on this topic and it was found that any injector configuration producing a strong recirculation zone, also produce stable combustion. This is thought to be due to the fact that the recirculation zone allows pre-heating of the oxidizer before being injected into the combustion port and also promotes mixing of propellants at the entrance of the fuel grain, thus reaching a good flame holding at the grain entry. Moreover, a good injector has to move the frequency of the vortex shedding away from that of the fuel-production oscillations or to reduce the amplitude of the vortex shedding, so that the unsteady heat release cannot be triggered by vortex shedding. In this research different kind of injectors were used as listed in Table 1.

Table 1: Overview of injectors used during the experimental campaign

Injector	2α [°]	L_{inj}/D_{inj} [−]	**Inclined holes**	**Straight holes**
Axial Showerhead No.1	0	6	0	48
Axial Showerhead No.2	0	6	0	42
Axial Showerhead No.3	0	6	0	20
Axial Showerhead No.4	0	3	0	22
Impingement No. 1	30	4.5	10	0
Impingement No. 2	30	6	16	0
Swirl+Axial	0	3 (Swirl)/3.15 (Axial)	3	8

4. Experimental Setup

The test bench M11.5 at the DLR Lampoldshausen is mainly designed to account for student use. It allows the operator to carry out the burning of the samples with safety and reliability, setting all the parameters of the burning test from a control room.

4.1 Test Article

Two different test articles were used during the experimental campaign. The main combustion chamber for both engines consists of a cylindrical central section and two square end caps. The central body has an outer diameter of 75 mm and a length of 145 mm. The whole chamber has a length of 22 cm and 27 cm respectively for the first and second engine and both deliver a thrust of about 500 N and a burning time of about 5 s. The chamber pressure is approximately 30 bar and the oxidizer to fuel ratio O/F selected lies around 6-7. The whole combustion chambers are made of aluminium, which has high strength and corrosion resistance. The interior of the aluminium casing is protected from the hot combustion gases of up to 3000 K by an ablative layer of PERTINAX, a composite material from paper and a phenol-formaldehyde synthetic resin, which can withstand high temperatures for about 15 s. Both test articles have a convergent-divergent graphite nozzle with an expansion ratio of about 5 and a conic shape. Some diaphragms with different geometries were used during the test campaign in both engine configurations. They were placed at the end of the fuel grain to improve mixing of the propellants and thereby increase the combustion efficiency. The ignition system is an electrically-initiated pyrotechnic igniter.

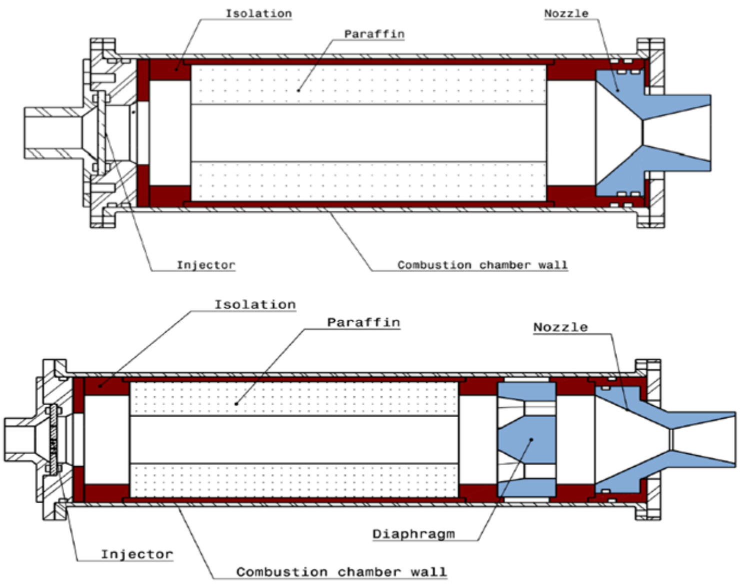

Figure 2: Cross section of the test articles

4.2 Instrumentation and Measurement

For temperature measurements, type K thermocouples are placed on the external wall of the combustion chamber and of the nozzle. They have a sensitivity of approximately 41 $\frac{\mu V}{°C}$ and their temperature measurement range is about from 0 °C to +600 °C.

Some piezoresistive pressure transducers from *Sensortechnics* are used in order to measure the pressure inside the chamber, in the oxidizer tank and upstream of the injector. The combustion chamber and the injector pressure sensors have a measurement range from 0 bar to 70 bar. The tank pressure sensor has a measurement range of 0-100 bar. Their relative error is 0.1% with respect to the measured value.

For measuring the instantaneous thrust, an *Althen* strain-gauge load cell is used. Its measurement range is 0-5000 N and it has an accuracy of 0.1% of the measured value. Its temperature operating range is from -55 °C to +120 °C and the maximum allowable load is 150% FS.

The oxidizer mass flow rate is measured using a Coriolis E+H flow meter. It has a measurement range of 0-5 $\frac{kg}{s}$ and a relative error of 0.25% with respect to the measured value. The Coriolis flow meter allows to measure simultaneously the mass flow, the density and the temperature of the oxidizer.

An overview of the sensors specifications is given in Table 2.

Table 2: Sensors specifications

Sensor	**Producer**	**Measurement Range**	**Accuracy**
Chamber Pressure	Sensortechnics	0-70 bar	0.1 %
Injector Pressure	Sensortechnics	0-70 bar	0.1 %
Tank Pressure	Sensortechnics	0-100 bar	0.1 %
Thermocouples	-	0-600 °C	-
Coriolis	Endress+Hauser	0-5 $\frac{kg}{s}$	0.25 %
Load Cell	Althen	0-5000 N	0.1 %

4.3 Feed System

The feed system is composed of a nitrous oxide feed line, control valves and the oxidizer tank. The plumbing and instrumentation diagram (P&ID) is shown in Figure 3.

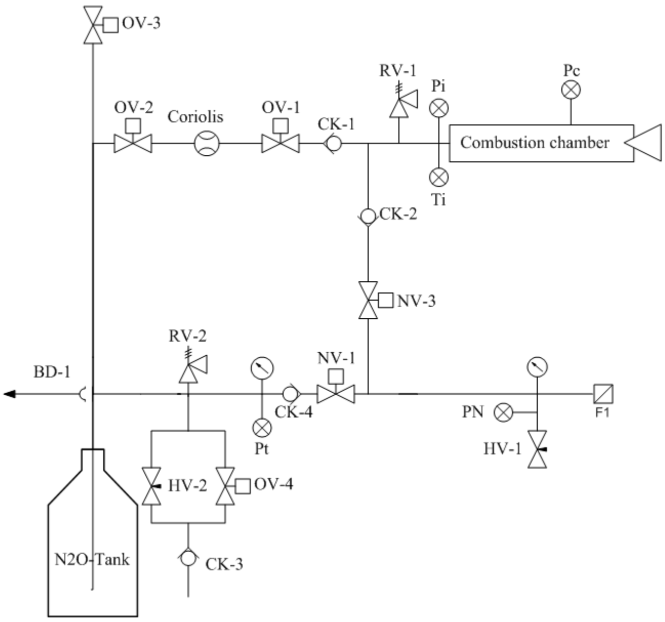

Figure 3: Plumbing and Instrumentation Diagram of the test facility

Although nitrous oxide is a self-pressurizing gas, additional pressurization is provided by N_2 in order to keep N_2O at a pressure considerably above the vapour pressure to avoid cavitation and two-phases flow in the feed line. The oxidizer pressure in the tank is about 55 bar at the beginning of the burning test. The filling of the N_2O run tank is done by remote control.

4.4 Control System and Data Acquisition

The test sequence is controlled remotely and executed via a National Instruments LabVIEW interface. The order and timing of operations is pre-programmed into an automated test fire sequence, thus ensuring a repeatable testing procedure. Burn times are set for each test based on the expected regression rate and initial port diameter of the fuel grain. About 4 seconds before the opening of the oxidizer valve the N_2O tank gets pressurized. Igniter firing occurs 0.5 seconds before the opening of the oxidizer valve. After the scheduled burning time (2-5 seconds depending on the test conditions), the oxidizer valve is closed and the lines and the chamber are purged with N_2. A NI PXI measurement system is used for data acquisition.

5. Propellant Characteristics

5.1 Tested Fuels

The fuels used for the test campaign are four different paraffin waxes, both in pure form and with additives in order to modify mechanical, rheological and burning properties. Their properties, given from the manufacturer, are reported in Table 3. Types 6003 and 6805 are pure paraffin waxes. Type 0907 is a micro-crystalline wax. Type 1276 is a formulation based on waxes and different additives inserted by the manufacturer in order to increase the mechanical properties of the pure paraffin [18, 19].

Paraffin-based fuels are characterized by a phenomenon called *entrainment*. It is based on the formation of a thin melt layer on the fuel surface from where liquid droplets are entrained by the oxidizer and the combustion products fluxes. Droplet formation is caused by liquid layer instabilities, which result from the high shear stress produced by the high velocity gas flow in the port [10]. This leads to a higher regression rate (3 to 6 times higher than conventional fuels) for two main reasons: droplets do not absorb the heat of vaporization and the blocking effect on the convective heat transfer is decreased. On the other hand, these *liquefying fuels* have some disadvantages such as low tensile strength and shrinkage which makes their manufacturing difficult. In order to increase the mechanical properties of the paraffin some additives are added to the fuel formulation.

For the ballistic tests all the samples were blackened in order to limit radiation effects to the fuel surface during combustion. Generally the amount of blackening additive was about 1% so that it has a negligible impact on the performance. Four different additives were chosen in order to improve the mechanical properties of the paraffin samples. Stearic acid (SA) was used in combination with paraffin 6003 and 6805. A nanoclay material from the manufacturer Byk and two polymers with a melting temperature similar to the paraffin samples were used in combination with 6805 [17].

Sasol Wax	**Congealing Point** [°C]	**Oil Content** [%]	**Viscosity at 100°C** [mm^2/s]	**Penetration at 25°C** [$1/10mm$]
6003	60-62	0-0.5	-	17-20
0907	83-94	0-1	14-18	4-10
6805	66-70	0-1	6-8	16-20
1276	64-68	-	880-920	8-13

Table 3: Wax properties declared by the manufacturer [18, 19]

5.2 Tested Oxidizer

The oxidizer used for the test campaigns is nitrous oxide, commonly known as laughing gas, whose chemical formula is N_2O. It is used as oxidizer in rocket engines because it is non-toxic, storable and non-explosive at room temperature, self-pressurizing (high vapour pressure), relatively safe and easy to handle [11, 12, 13, 14]. Its high density and low storage pressure (when maintained at low temperature) make it competitive with stored high-pressure gas system. The self-pressurization allows for a simple oxidizer feed system with no additional pressurizing gas or even pumps.

6. Experimental Results

6.1 Regression Rate Analysis

Experimental data of single tests were analyzed as explained in Sec. 2. The time-space averaged regression rate and oxidizer mass flux were computed, together with the error bars for the regression rate. Then the regression rate curves for each paraffin formulation were plotted by using a power law interpolation of single tests. The curves for the tested fuel formulations with showerhead injectors are shown in Fig 4. Literature data of HTPB, HDPE and another paraffin-based fuel in combination with different oxidizers are also shown in order to compare the results.

It is possible to note that all the fuel formulations tested during the test campaign in combination with nitrous oxide show a regression rate that is higher than that of polymeric fuels in combination with liquid oxygen. This is due to the additional mass transfer caused by the entrainment, which leads to an increase in the fuel surface roughness and to a reduction of the effective heat of gasification and blocking factor in the boundary layer. Moreover, it is possible to see that tests performed with paraffin 6003 and 6805 both with 10% of stearic acid show the highest regression rates. They also have the lowest viscosity, which means higher mass flux entrained from the fuel surface. In fact, the regression rates are decreasing as the viscosity values of the fuel samples are increasing, as it was shown in detail in Kobald et al. [17]. The viscosity data measurements of these paraffin formulations are also shown in [17]. The mixture with 5% of polymer show a regression rate which is lower with respect to that of other paraffin-based mixtures but still higher than that of polymeric fuels.

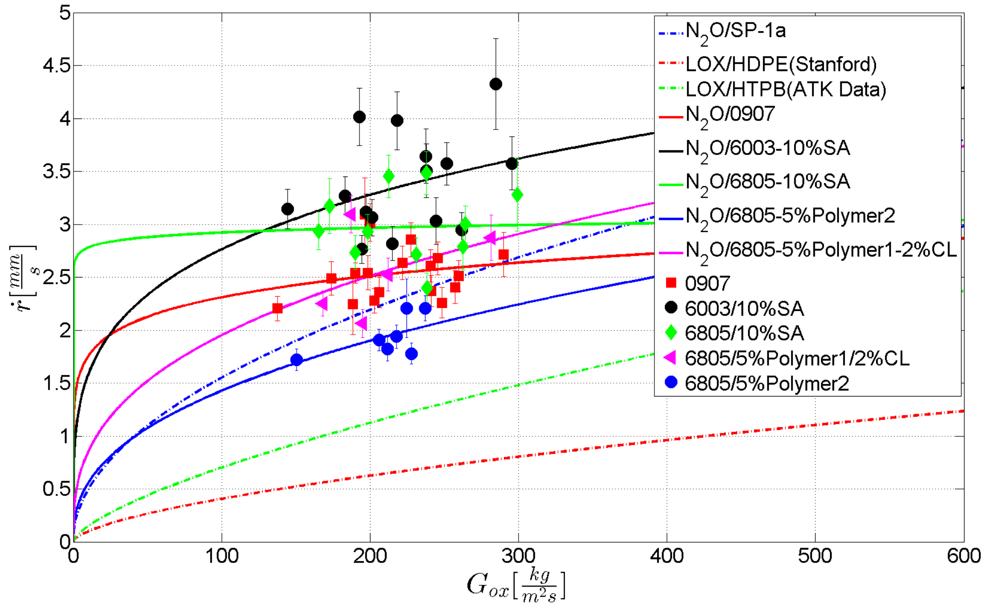

Figure 4: Regression rate curves

Regarding the injector configuration: changing from the axial to the impingement 1 (see Table 1: note that impingement 1 and 2 have the same holes area but different number of holes), a strong increase of the regression rate can be seen. This is due to a more uneven distribution of the oxizider and to an increase in the local N_2O impinging on the fuel surface. The space-time averaged regression rate values for the mixture 6805+10%SA with axial and two different impingement injectors are shown in Figure 5.

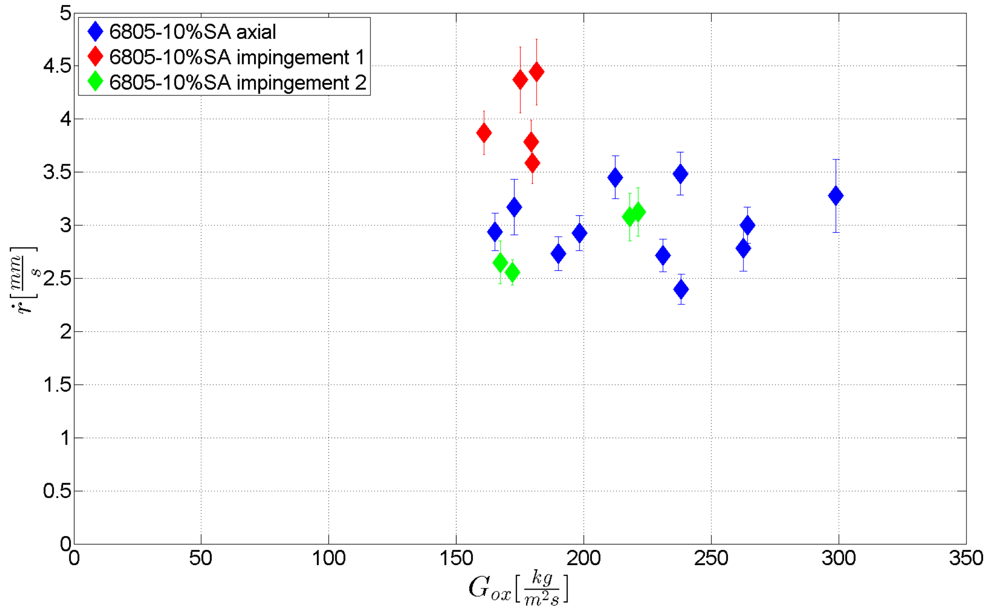

Figure 5: Regression rate curves with axial and impingement injectors (6805+10%SA)

It is important to note that configurations with and without diaphragm show the same regression rate since it is placed at the end of the fuel grain.

6.2 Engine Performance Analysis

Average engine c^* efficiencies and their error bars are computed as explained in Sec. 2 and reported in Fig 6.

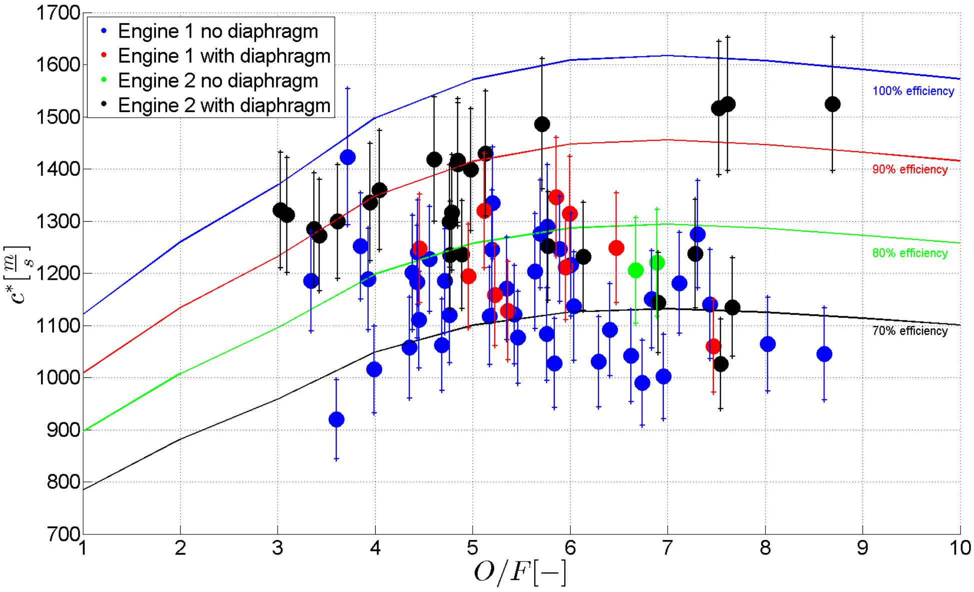

Figure 6: Characteristic velocity vs. mixture ratio

Higher combustion efficiencies are reached using the engine with the longer post-combustion chamber, since it enhances the mixing of the combustion products and increases the residence time. In order to reach a more complete mixing without increasing too much the engine volume and dry mass, the post-combustion chamber was used in combination with a perforated mixing plate located at the end of the fuel grain. Different diaphragm geometries were tested in both engines and an increase in the combustion efficiency with respect to configurations without diaphragms was observed. This happens because the diaphragm forces the mixing of the oxidizer with the fuel and combustion products generated before it, thus enhancing the local completeness of the combustion [15]. The price of a higher c^* efficiency is a pressure drop across the diaphragm that reduces the chamber pressure available for the expansion in the nozzle. Moreover, higher combustion efficiencies are reached with the impingement injector due to a better atomization of the oxidizer. Finally, the combustion efficiency tends to increase with decreasing the mixture ratio since, with fuel-rich conditions, a more complete combustion of the oxidizer is accomplished. Only with the mixture 6805+5%Polymer2 a high combustion efficiency is achieved also at higher mixture ratio, since it shows a lower burning rate. The efficiencies of the specific impulse show the same trend as the combustion efficiencies (Fig. 7).

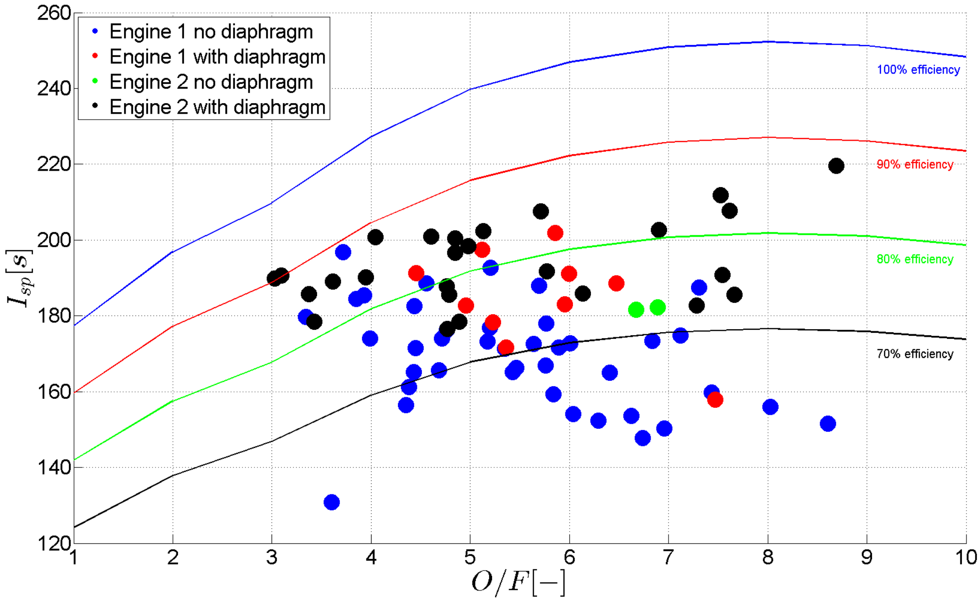

Figure 7: Specific Impulse vs. mixture ratio

6.3 Combustion Stability Analysis

A frequency analysis of the chamber pressure signal was performed with MATLAB® using the Signal Processing Toolbox. Combustion stability was evaluated by using Fast-Fourier Transformations, spectrograms and "Pwelch" plots. All the theoretical frequencies were computed using the formula given by Karabeyoglu et al. [9] and Carmicino [8] and they are compared with the experimental frequencies showing magnitude peaks in the plots (see Section 2).

In almost every test, the intrinsic low frequency instability was present even if the oscillations were never so high to cause an unstable burning behaviour. It varies in a range that goes from 70 Hz to 140 Hz depending on the injector geometry and on the presence of the diaphragm. In some tests, a peak in correspondence of the vortex shedding frequency in the pre-chamber is shown. Its theoretical value lies between 30 Hz and 90 Hz. In a few tests it is possible to see also the Helmholtz frequency and the vortex shedding in the post-chamber, whose values vary respectively between 300-600 Hz and 200-1000 Hz. The longitudinal frequency, which is around 2500 Hz for the smaller chamber and 2000 Hz for the longer one, could not be measured with the instrumentation used for the majority of the tests since the pressure sensor had a sampling frequency of 1000 Hz. For the last tests a new pressure sensor with a sampling frequency of 20 kHz was used, so that the acoustic mode of the chamber was seen in the spectrogram.

Tests 36 and 86 were performed under comparable operating conditions but different injector configurations. In test 36 the axial showerhead injector number 2 was used, while in test 86 it was replaced by the impingement injector number 2. The chamber pressure time traces, spectrograms and FFT can be seen respectively in Fig. 8, 9 and 10. Test 36 shows chamber pressure oscillations with an amplitude of approximately 5.4% of the mean pressure. These oscillations are, in general, caused by the unsteady heat release in the combustion chamber. According to Carmicino [8], this is due to a poor flame holding and atomization of the oxidizer at the grain entry or the vortex shedding of the oxidizer flow after the sudden expansion from the injector to the fuel grain. The unsteady heat release in the pre-chamber triggers acoustic modes, thus enhancing the heat flux to the fuel surface and triggering the intrinsic low frequency instability [8]. It is possible to note a typical feed system coupled instability behaviour, due to a low injector pressure drop. At the end of the combustion the nozzle cracked, thus increasing the throat diameter. This causes a decrease in the chamber pressure and an increase in the injector pressure drop, thus leading to a stable combustion. In the spectrogram strong oscillations at about 100 Hz, which are in the range of the intrinsic low frequency, can be clearly seen, together with other oscillations at around 200 Hz and 300 Hz which could be the second and third modes of this instability. Lower frequencies oscillations, associated with the vortex shedding in the pre-chamber, are present at around 50 Hz at the beginning of the combustion. The oscillations between 350 and 400 Hz, which are present during the entire burning process, are linked to the Helmholtz mode. An oscillating band with decreasing frequency, associated with the vortex shedding in the post-chamber, can be seen between 500 and 450 Hz. It is not possible to see the acoustic modes due to the low sampling frequency of the pressure transducer. Test 86 shows a stable combustion without strong oscillations. In the spectrogram only a low-intensity oscillating band at about 100 Hz can be seen, which is in the range of the low frequency instability. This indicates that the unsteady heat release in the chamber is suppressed and the acoustic modes are not triggered.

From the experimental data it is possible to note that no strong instabilities were observed during the tests: oscillations of the chamber pressure remain bounded in a range from less than 1% to 9% of the mean pressure value. Higher oscillations are associated with the presence of the diaphragm at the end of the fuel grain and injectors with improper atomization behaviour. Lower oscillations are observed for tests without the diaphragm and with the impingement injector. In particular, it is possible to note that tests using an impingement injector show a very stable combustion with oscillations lower than 1%, also in presence of a diaphragm. For example, tests using 6805+10%SA show oscillations of almost 9% for the configuration with the diaphragm and the 48 holes axial injector, while they become 0.8% for the configuration with the diaphragm and the impingement injector. This is most likely due to the improved atomization behaviour of impingement injector with respect to the axial one. Moreover, oscillations also depend on the conditions of the oxidizer. From the results of other tests it was seen that the stability is improved by a high vapour pressure of N_2O in the combustion chamber. In fact, when the local pressure in the chamber is below the vapour pressure, the N_2O is likely to flash vaporize.

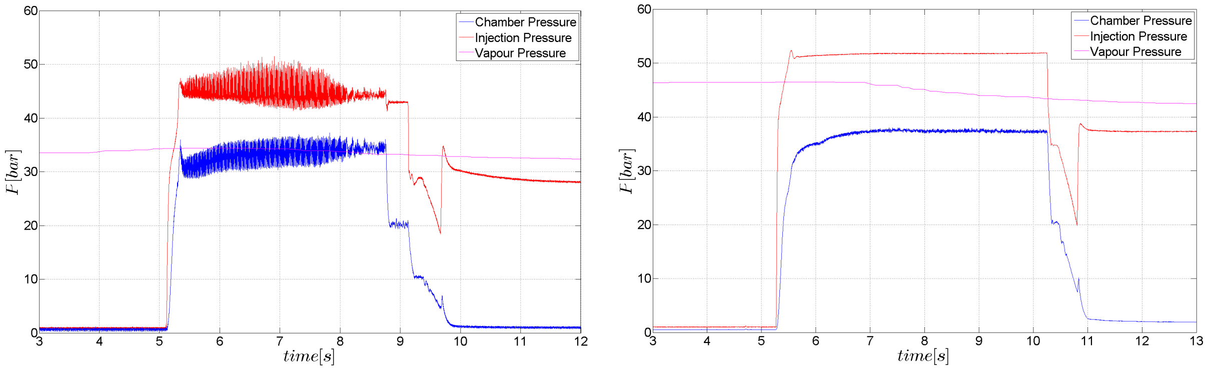

Figure 8: Pressure time trace tests 36 (left) and 86 (right)

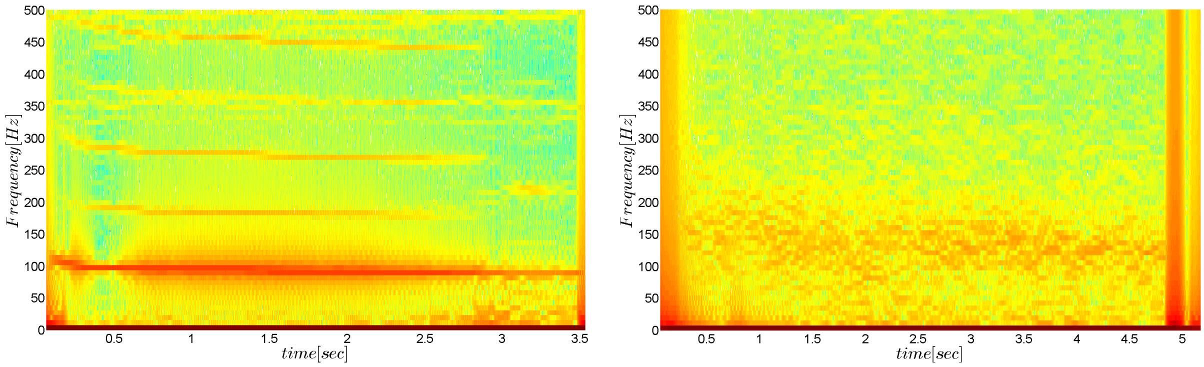

Figure 9: Chamber pressure spectrogram tests 36 (left) and 86 (right)

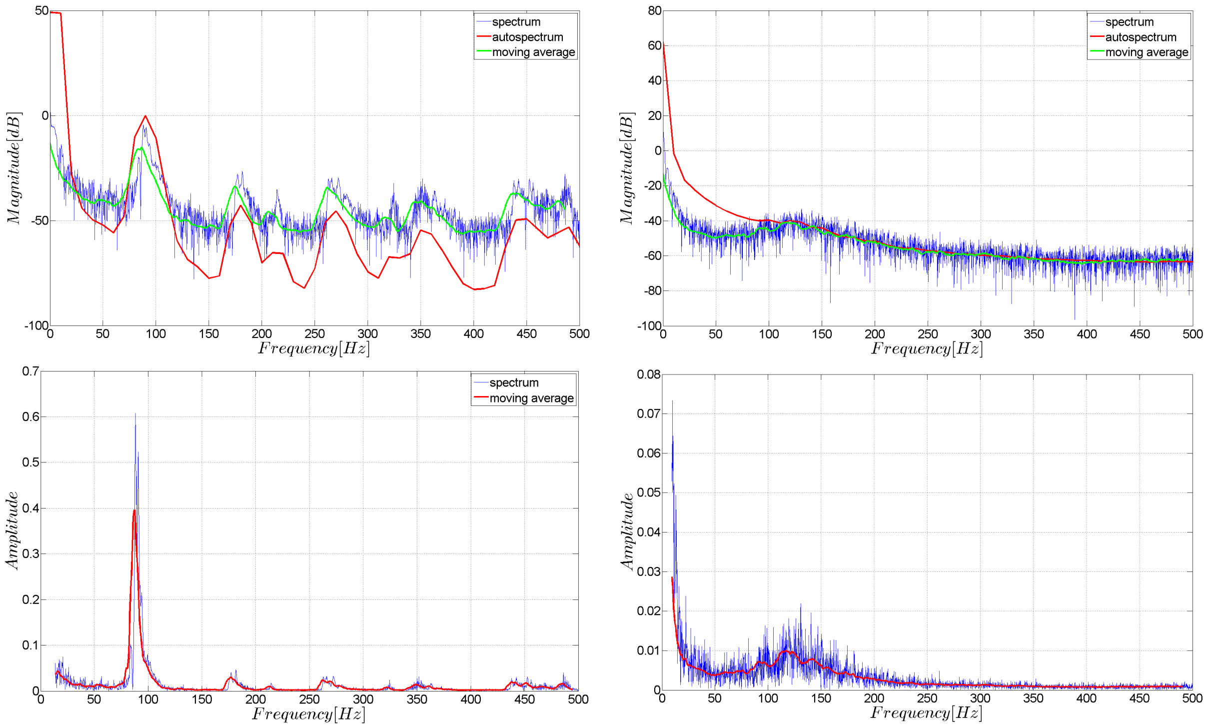

Figure 10: Chamber pressure spectrum tests 36 (left) and 86 (right)

7. Conclusion

A test campaign of 86 tests was carried out using a 500 N engine with different paraffin-based fuels and nitrous oxide. All the regression rates and performance parameters were obtained by a time averaging process over the burning time. Combustion stability was evaluated by using Fast-Fourier Transformations, spectrograms and power spectral densities of the chamber pressure signal.

Concerning the regression rate, it was observed that paraffin-based fuels show a higher regression rate with respect to conventional polymeric fuels. In particular, paraffin waxes tested during our test campaign in combination with nitrous oxide show regression rates which are 3 to 6 times higher than those of HTPB in combination with liquid oxygen. Moreover an increase in the fuel viscosity results in a decreased regression rate, since a lower mass flux is entrained from the fuel surface. The regression rate is also influenced by the injector configuration: tests performed with the impingement injector with low number of holes show higher regression rates with respect to tests that use the axial ones. Engine configurations with a diaphragm placed at the end of the fuel grain do not show any increase in the regression rate, since the flow goes directly from the diaphragm to the nozzle.

For what concerns the engine performance, it was found that the combustion efficiency increases up to 25% when a diaphragm is placed at the end of the fuel grain. This is due to the enhanced mixing of the oxidizer with the fuel and combustion products generated by the diaphragm. Moreover tests performed with the impingement injector show combustion efficiencies which are up to 24% higher than those of tests using the axial ones. This is caused by the improved atomization behaviour of the impingement injector and by the increase in the turbulence level in the chamber which leads to a better mixing of propellants.

No strong instabilities were observed during the tests: oscillations of the chamber pressure remain bounded in a range from less than 1% to 9% of the mean pressure value. Higher oscillations are associated with the presence of the diaphragm at the end of the fuel grain and injectors with poor atomization performance. Lower oscillations are observed for tests without the diaphragm and with the impingement injector, which promotes a better oxidizer atomization, propellant mixing and flame holding, thus suppressing the unsteady heat release in the chamber.

8. Acknowledgements

Since September 2012 the HyEnD-STERN project is sponsored by the DLR Space Administration with funding from the Federal Ministry for Economic Affairs and Energy (BMWI) at the Institute of Space Systems at the University of Stuttgart, under the grant number 50RL1254. The experimental tests have been performed in cooperation with the Institute of Space Propulsion at the DLR Lampoldshausen, at test complex M11.5. The support of the DLR Lampoldshausen and its department of propellants is greatly acknowledged. The authors would like to thank all the students, individuals, institutes and companies who supported the presented work in several manners. A special thanks to Dr. Thomas Wegmann at the Institute of Space Systems for his excellent administrative support. A complete list of our supporters is presented on www.hybrid-engine-development.de.

References

[1] M. Kobald, H. Moser, A. Bohr, and S. Mielke, Development and Optimization of a Hybrid Rocket Engine, *Deutscher Luft- und Raumfahrtkongress*, Aachen, Deutschland, 2009.

[2] K. Lappoehn, D. Regenbrecht, and D. Bergmann, STERN A Rocket Programme for German Students, *5th European Conference for Aeronautics and Space Sciences*, Munich, Germany, 2013.

[3] M. Kobald, C. Schmierer, and A. Petrarolo, Test campaign of a 10000 N Hybrid Rocket Engine, *6th European Conference for Aeronautics and Space Sciences*, Krakow, Poland, 2015.

[4] G.A. Marxman, M. Gilbert, Turbulent Boundary Layer Combustion in the Hybrid Rocket, *9th International Symposium on Combustion*, The Combustion Institute, 1963.

[5] M. A. Karabeyoglu, B.J. Cantwell, G. Zilliac, Development of Scalable Space-Time Averaged Regression Rate Expression for Hybrid Rockets, *41st AIAA/ASME/SAE/ASEE Joint Propulsion Conference and Exhibit*, AIAA Paper 2005-3544, July 2005.

[6] G.P. Sutton, O. Biblarz, *Rocket Propulsion Elements*, *8th Ed.*, John Wiley & Sons Inc., 2010.

[7] M. Kobald, T. Willerding, A. Schindler, M. Kott, M. Hahn, H. Ciezki, S. Schlechtriem, Injection Effects in Hybrid Rocket Engines, *Space Propulsion Conference*, Bordeaux, 2012.

[8] C. Carmicino, Acoustics, Vortex Shedding and Low-Frequency Dynamics Interaction in an Unstable Hybrid Rocket, *Journal of Propulsion and Power*, Vol. 25, No. 6, November-December 2009.

[9] M. A. Karabeyoglu, S. De Zilwa, B.J. Cantwell, G. Zilliac, Modeling of Hybrid Rocket Low Frequency Instabilities, *Journal of Propulsion and Power*, Vol. 21, No. 6, November-December 2005.

[10] M.A. Karabeyoglu, D. Altman, B.J. Cantwell, Combustion of Liquefying Hybrid Propellants: Part1, General Theory, *Journal of Propulsion and Power*, Vol.18, No. 3, May-June 2002.

[11] G. Zilliac, B.S. Waxman, J. Dyer, M.A. Karabeyoglu, B.J. Cantwell, Peregrine Hybrid Rocket Motor Ground Test Results, *48th AIAA/ASME/SAE/ASEE Joint Propulsion Conference and Exhibit*, AIAA Paper 2012-4017, 30 July-01 August 2012.

[12] K. Lohner, J. Dyer, E. Doran, Z. Dunn, G. Zilliac, Fuel Regression Rate Characterization Using a Laboratory Scale Nitrous Oxide Hybrid Propulsion System, *42nd AIAA/ASME/SAE/ASEE Joint Propulsion Conference and Exhibit*, AIAA Paper 2006-4671, 9-12 July 2006.

[13] E. Doran, J. Dyer, K. Lohner, Z. Dunn, B.J. Cantwell, G. Zilliac, Nitrous Oxide Hybrid Rocket Motor Fuel Regression Rate Characterization, *43rd AIAA/ASME/SAE/ASEE Joint Propulsion Conference and Exhibit*, AIAA Paper 2007-5352, 8-11 July 2007.

[14] J. Dyer, E. Doran, Z. Dunn, K, Lohner, C. Bayart, A. Sadhwani, Design and Development of a 100 km Nitrous Oxide/Paraffin Hybrid Rocket Vehicle, *43rd AIAA/ASME/SAE/ASEE Joint Propulsion Conference and Exhibit*, AIAA Paper 2007-5362, 8-11 July 2007.

[15] M. Grosse, Effect of a Diaphragm on Performance and Fuel Regression of a Laboratory Scale Hybrid Rocket Motor Using Nitrous Oxide and Paraffin, *45th AIAA/ASME/SAE/ASEE Joint Propulsion Conference and Exhibit*, AIAA Paper 2009-5113, August 2009.

[16] E. Doran, J. Dyer, K. Lohner, Z. Dunn, B.J. Cantwell, G. Zilliac, Nitrous Oxide Hybrid Rocket Motor Fuel Regression Rate Characterization, *43rd AIAA/ASME/SAE/ASEE Joint Propulsion Conference and Exhibit*, AIAA Paper 2007-5352, 8-11 July 2007.

[17] M. Kobald, C. Schmierer, H. Ciezki, S. Schlechtriem, E. Toson, L. T. De Luca, Evaluation of Paraffin-based Fuels for Hybrid Rocket Engines, *50th AIAA/ASME/SAE/ASEE Joint Propulsion Conference and Exhibit*, AIAA Paper 2014-3646, 28-30 July 2014.

[18] M. Kobald, E. Toson, H. Ciezki, S. Schlechtriem, S. Di Betta, M. Coppola, L.T. De Luca, Rheological, optical and Ballistic Investigations of Paraffin-Based Fuels for Hybrid Rocket Propulsion Using a 2D Slab-Burner, *5th European Conference for Aeronautics and Space Sciences (EUCASS)*.

[19] E. Toson, M. Kobald, S. Di Betta, L.T. De Luca, H. Ciezki, S. Schlechtriem, Rheological and Ballistic Investigations of Paraffin-Based Fuels for Hybrid Rocket Propulsion Using a 2D Radial Micro-Burner, *5th European Conference for Aeronautics and Space Sciences (EUCASS)*.

Abbreviations

DLR	Deutsches Zentrum für Luft- und Raumfahrt (German Aerospace Center)
HEROS	Hybrid Experimental Rocket Stuttgart
HyEnD	Hybrid Engine Development, DGLR student group
HyRES	Hybrid Rocket Engine Stuttgart
HDPE	High-density Polyethylene
HTPB	Hydroxyl-terminated Polybutadien
IRS	Institut für Raumfahrtsysteme, Universität Stuttgart (Institute for Space Systems, University of Stuttgart)
MIRAS	Micro Rakete Stuttgart (demonstrator rocket)
MORABA	Mobile Raketenbasis (DLR sounding rocket division)
STERN	STudentische Experimental RaketeN (Student Experimental Rockets, educational programme of DLR)

Nomenclature

A_t	nozzle throat area
C_d	discharge coefficient
D_f	final space-average port diameter
D_i	initial port diameter
D_t	nozzle throat diameter
E_{D_i}	measurement error on the initial port diameter
E_{D_f}	measurement error on the final port diameter
E_t	measurement error on the burning time
$E_{\dot{m}_{Ox}}$	measurement error on the oxidizer mass flow
F	thrust
G	propellants mass flux
G_{Ox}	oxidizer mass flux
I_{sp}	specific impulse
L	total combustion chamber length
L_{fuel}	fuel grain length
OF	mixture ratio
P_c	chamber pressure
Sr	Strouhal number
V	combustion port total volume
a, n, m	ballistic coefficients
c	average sped of sound in the chamber
c^*	characteristic velocity
l	nozzle length
m_{fuel_i}	initial fuel mass
m_{fuel_f}	final fuel mass
$\dot{m}_{Ox}$	oxidizer mass flow
$\dot{m}_f$	fuel mass flow
$\dot{r}$	regression rate
t_b	burning time
ρ_{fuel}	fuel density